Journal of Catalysis **199,** 236–246 (2001)
doi:10.1006/jcat.2001.3163, available online at http://www.idealibrary.com on IDEAL®

Different Functions of the Noble Metals Added to Cobalt Catalysts for Fischer–Tropsch Synthesis

Noritatsu Tsubaki,[1] Shouli Sun, and Kaoru Fujimoto

Department of Applied Chemistry, School of Engineering, The University of Tokyo, Hongo 7-3-1, Bunkyo-ku, Tokyo 113-8656, Japan

Received August 21, 2000; revised January 4, 2001; accepted January 4, 2001; published online March 21, 2001

The influence of the addition of very small amounts of Ru, Pt, and Pd to supported cobalt catalysts, which were prepared by mixing cobalt nitrate and cobalt acetate, has been investigated for the Fischer–Tropsch synthesis. Catalysts containing 10 wt% Co (5 wt% from cobalt nitrate and 5 wt% from cobalt acetate) and a very small amount of Ru, Pt, or Pd were prepared by coimpregnation. The weight ratio of M to total Co was 1/50 (M = Ru, Pt, Pd). At $T = 513$ K, $P = 1.0$ MPa, $H_2/CO = 2$, and $W/F = 5$ g-cat. h mol^{-1}, CO hydrogenation rates followed the order RuCo > PdCo > PtCo > Co. The addition of a small amount of Ru to Co/SiO_2 catalyst increased the catalytic activity and the reduction degree remarkably. The turnover frequency (TOF) increased but the CH_4 selectivity was unchanged. However, added Pt or Pd catalyst exhibited higher CH_4 selectivity. Although Pt and Pd exerted hardly any effect on the degree of cobalt reduction, they promoted cobalt dispersion and decreased the TOF. Characterization of these bimetallic catalysts suggested that different contacts between Co and Ru, Pt, or Pd existed. Ru was enriched on cobalt but Pt, or Pd dispersed well in the form of Pt–Co or Pd–Co alloy.

Key Words: **cobalt catalyst; noble metal; Fischer–Tropsch synthesis; CO hydrogenation.**

INTRODUCTION

Cobalt-based catalysts are known to be effective in CO hydrogenation (1, 2). Recent studies indicated that the Fischer–Tropsch synthesis (FTS) activity of Co catalysts depends solely on the number of active sites located on the surface of crystalline metal formed by the reduction. The number of active sites was determined by the Co particle size, loading amount, and reduction degree (3, 4).

Synthesis of highly dispersed Co catalysts requires the initial formation of very small CoO or Co_3O_4 crystallites. The formation of such small oxide clusters requires strong interactions between the support and Co precursor, but in turn such strong interactions generally lower the degree of reduction of such precursors to Co metal (5). Silica–cobalt carboxylate support–precursor pairs lead to very small CoO_x particles, which are reduced completely only above 1000 K and form sintered metal particles (6). Silica–cobalt nitrate pairs form CoO_x particles of intermediate size during nitrate decomposition; these crystallites can be reduced at 673 K in flowing H_2.

Highly dispersed cobalt catalysts derived from cobalt carbonyl clusters or cobalt acetate are active in the formation of oxygenates by CO hydrogenation (6–8). The present authors have reported that the catalysts prepared by mixing cobalt nitrate and cobalt acetate had higher activity than the catalysts prepared from a single precursor and the main products were paraffins and olefins (9, 10). The degree of reduction of the catalyst prepared from mixed precursors was remarkably higher than that of catalysts prepared from cobalt acetate as the latter could not be reduced to metallic cobalt at a relatively low temperature.

A number of investigations have been focused on the noble metal as the promoter for cobalt-supported catalysts. Zsoldos *et al.* (11) studied Co–Pt catalysts with high Pt/Co ratios. Their findings include a Pt-assisted mechanism for reduction of Al_2O_3-supported Co catalysts and a stabilization of Co ions on the Al_2O_3 surface. Iglesia *et al.* (12) showed that the presence of Ru in supported cobalt catalysts not only enhanced the reduction of cobalt oxide but also inhibited carbon deposition during FTS. Guczi *et al.* (13, 14) studied Co–Pt catalysts with high Pt/Co ratios. Pt/Al_2O_3 with high Pt/Co ratio catalysts tended to favor the formation of oxygenate (13). Schanke *et al.* (15) studied Co–Pt catalysts with low Pt/Co ratios and found that the selectivity was not influenced by the presence of Pt, but the cobalt oxide reducibility and dispersion were increased significantly for Co/Al_2O_3 catalysts. However, on SiO_2-supported Co catalysts, the presence of Pt did not influence the final extent of reduction and increased the dispersion slightly (15).

In order to obtain higher reduction degree and higher catalytic activity, the reduction behavior and structural features of the Co/SiO_2 prepared by mixing cobalt nitrate and cobalt acetate, promoted by trace amount of Ru, Pt, or Pd, were investigated. The effect of added noble metals on

[1] To whom correspondence should be addressed. Present address: Dept. of Applied Chemistry, School of Engineering, Toyama University, Toyama, Japan, 930-8555.

0021-9517/01 $35.00

the FTS properties of cobalt catalysts prepared by mixing cobalt nitrate and cobalt acetate was elucidated here.

EXPERIMENTAL

Catalyst Preparation

Supported catalysts containing 10 wt% Co (5 wt% from cobalt nitrate and 5 wt% from cobalt acetate) and very small amount (0.2 wt%) of Ru, Pt, or Pd were prepared by incipient wetness coimpregnation of the supports with aqueous solutions of $Co(NO_3)_2 \cdot 6H_2O$ and $Co(CH_3COOH)_2 \cdot 4H_2O$ (Kanto Chemicals Co.), as well as $Pd(NH_3)_2(NO_2)_2$, $Pt(NH_3)_2(NO_2)_2$, and $Ru(NO_3)_3$ (Tanaka Noble Metal Co.). The weight ratio of M to total Co was 1/50 (M = Ru, Pt, Pd). The molar ratio of M to total Co was between 0.61% and 1.16%. The support was commercially available silica gel (ID gel, Fuji Davison; specific surface area, 270 $m^2\ g^{-1}$; pore volume, 1.22 $cm^3\ g^{-1}$; average pore diameter, 8.7 nm). The catalyst precursors were dried in air at 393 K for 12 h, and then calcined in air at 723 K with a ramping rate of 3 K min^{-1} for 2 h. After calcination, the catalysts were activated in flowing hydrogen at 673 K for 10 h; the temperature ramping rate was again 3 K min^{-1}. Finally, the catalysts were passivated by 1% oxygen in nitrogen.

CO Hydrogenation

CO hydrogenation was carried out in a flow-type semibatch autoclave slurry-phase reactor with an inner volume of 80 ml. The passivated catalyst (1.0 g, 80–100 mesh) and 20 ml of liquid medium (*n*-hexadecane) were loaded in the reactor. Before the reaction, reactant gas of 0.1 MPa was used to reduce the passivated catalyst again for 1 h at the same temperature as that used in FTS. Syngas flow rate in the reduction was 30 ml/min. During the reaction, the effluent gas released from the reactor was first cooled with a dry-ice trap, and then introduced to an online gas chromatograph equipped with Propak Q and active carbon columns for C_1–C_4, CO, and CO_2 analysis. The liquid products collected in the dry-ice trap and the products remaining in the slurry were combined and all of them were analyzed by gas chromatography with an SE-30 column. Argon was employed as an internal standard with a concentration of 3% in the feed gas. The standard reaction conditions were $P(\text{total}) = 1.0$ MPa, $H_2/CO = 2$, $W/F\ (CO + H_2 + Ar) = 5$ g h mol^{-1}, and $T = 513$ K.

Alcohols were not detected in the GC–MS experiment. After the experiment, the water phase of the collected FT products was analyzed but no alcohol was present.

Catalyst Characterization

An RINT 2400 (Rigaku) X-ray diffractometer instrument with monochoromatized CuK_α radiation was used for XRD measurements. The XRD spectra were measured under an atmosphere.

Chemisorption experiments were carried out in a static volumetric glass high-vacuum system. Research grade gases (H_2, 99.9995%; O_2, 99.99%; CO, 99.99%; Takachiho Co.) were used without further purification. Before adsorption of H_2 or CO, the catalysts, previously reduced by H_2 and passivated, were treated in H_2 at 673 K for 1 h, followed by evacuation. H_2 adsorption isotherms were measured at 373 K, as described in detail elsewhere (16). The CO chemisorption was conducted at room temperature. The reduction level was determined after reduction of the catalyst followed by O_2 titration at 673 K. The reduction percentage was calculated by assuming stoichiometric conversion of metallic Co to Co_3O_4 (17). For the chemisorption of the used catalyst, the wax on the catalyst surface was extracted by octane beforehand, in a reflux condensor at 323 K for 1 h. The used catalyst was then transferred to the vacuum line for chemisorption under the protection of N_2. The sample was evacuated for 3 h to remove octane before H_2 chemisorption.

Temperature-programmed surface reaction (TPSR) experiments were conducted in a hydrogen flow at a rate of 5 K min^{-1} from 298 K to 673 K, after removal of the physically adsorbed CO. Products such as CH_4, CO, and CO_2 were analyzed on a gas chromatograph equipped with a methanator and a flame ionization detector (FID).

Temperature-programmed reduction (TPR) experiments were carried out in a quartz microreactor. The gas stream, a mixture of 5% H_2 diluted by argon as reducing gas, was fed via a mass flow controller. After passing through reactor, the effluent gas was led through a 3 A molecular sieve trap to remove the produced water. The effluent gas was analyzed on a gas chromatograph with a thermal conductivity detector (TCD), with argon used as a reference. The reducing gas flow rate was 50 ml min^{-1}, and the temperature was raised at a rate of 7 K min^{-1} to 1073 K.

FTIR spectra were recorded in transmission mode (Nicolet Magna 550) with 2 cm^{-1} resolution using an MCT detector. About 30–40 mg of sample was pressed into a 10-mm-diameter self- supporting disk and put into a slit of the holder in an IR cell. The catalysts were reduced in the cell at 673 K for 1 h. CO of 200 Torr was adsorbed on the catalysts at room temperature for 10 min and then evacuated before the FTIR spectra of the CO adsorption were measured.

Transmission electron microscopy (TEM) images were taken on a JEM-2010F (JEOL) operated at 200 kV. A catalyst pellet was embedded into resin and cut by the microtome method (Leica Ultracut UCT). For elemental analysis of individual metal particles, a suitable sampling area was identified and photographed in the transmission mode and then the microscope was switched over to scanning transmission mode for energy dispersive spectroscopy (EDS).

The average particle size is estimated as $\sum n_i d_i^3 / \sum n_i d_i^2$. A 0.5-nm electron probe was focused on individual metal particles and X-ray counts were acquired for 100 s.

X-ray photoelectron spectroscopy (XPS) spectra were recorded using a VG ESCALAB 220 spectrometer with a MgK_α radiation source, where reduced sample could be prepared *in situ* without exposure to air. The C_{1s} photoemission line was taken as a reference to correct for electrostatic charging.

RESULTS

Catalytic Activity

Figure 1 shows the CO conversion and CH_4 and CO_2 selectivity as functions of Ru loading. It was found that the catalytic activity was determined apparently by the amount of Ru added. The catalytic activity showed an initial sharp increase with increasing Ru loading, reaching maximum at around 0.2% (absolute weight percent, Ru/(Ru + Co) = 1.16 mol%). The CH_4 selectivity did not show a meaningful change. The CO_2 selectivity increased slightly with Ru loading.

The catalytic activities of Ru-, Pt-, and Pd-promoted catalysts are summarized in Table 1. Although the activity of Co was 33.5%, the catalytic activity of RuCo catalyst was 72.3%. However, if the catalyst precursor was only cobalt nitrate and was also promoted by 0.2 wt% Ru, the catalytic activity was only 56.7%. According to Table 1, the degree of catalytic activity followed the order RuCo > PdCo > PtCo > Co > 0.2Ru. The activity of catalyst 0.2Ru itself was only 2.5% because of the low loading. It seems that ruthenium itself in RuCo catalyst did not contribute significantly to the activity of RuCo.

The catalyst promoted by Pd and Pt displayed higher methane selectivity than the catalyst promoted by Ru or Co only. The methane selectivity decreased in the order of PdCo > PtCo > RuCo, Co. Iglesia *et al.* reported that the catalyst prepared from cobalt nitrate only and promoted by Ru exhibited high C_5^+ selectivity and large chain growth probability (α) (12). But the catalyst prepared by mixing cobalt nitrate and cobalt acetate and that promoted by Ru, Pt, or Pd showed smaller chain growth probability. It was even smaller than that of the catalyst derived from the mixture of cobalt salts.

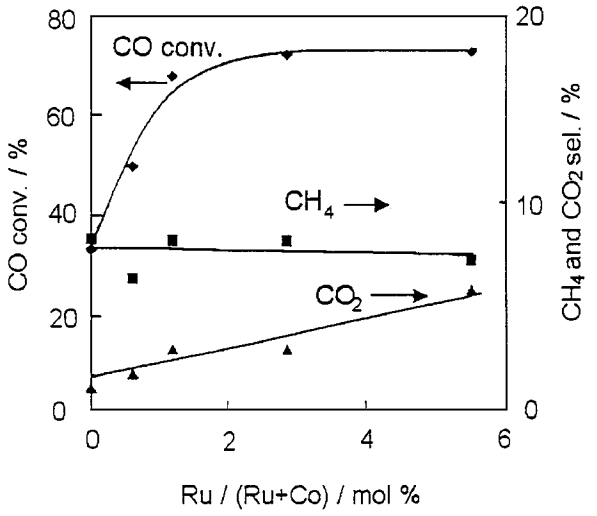

FIG. 1. Dependence of CO conversion, CH_4 selectivity, and CO_2 selectivity on the Ru loadings. Reaction conditions: 513 K, 1.0 MPa, W/F = 5 g-cat. h mol^{-1}, $H_2/CO = 1.77$.

TABLE 1

Catalytic Performance of Various Co (10 wt%)/SiO_2 Catalysts for CO Hydrogenation

Catalyst	CO conv./%	CH_4 sel./%	CO_2 sel./%	α	Cobalt–time yield[d] ($\times 10^4$ s^{-1})
Co[a]	33.5	8.89	1.27	0.83	1.86
RuCo[a]	72.3	8.81	3.32	0.76	4.02
PtCo[a]	49.5	13.78	9.48	0.75	2.75
PdCo[a]	57.9	17.76	4.79	0.75	3.22
Ru	2.5	4.81	0.14		0.14
RuCo[b]	56.7	6.25	2.18	0.88	3.15
Co[c]	29.8	6.58	1.64	0.86	1.66

Reaction conditions: 513 K, 1.0 MPa, $CO/H_2 = 1/2$, $W/F = 5$ g-cat. h mol^{-1}; total cobalt loading, 10 wt%.

[a] Catalyst precursor was a mixture of cobalt nitrate and cobalt acetate; the molar ratio of nitrate to acetate was 1, and the noble metal loadings were 0.2 wt%.

[b] 10 wt% Co (from cobalt nitrate) and 0.2 wt% Ru by coimpregnation.

[c] 10 wt% Co (from cobalt nitrate).

[d] Cobalt–time yield: moles of CO converted per total gram-atoms of Co per second.

TPR Behaviors of Various Catalysts

For the Co catalyst, the temperature of the first peak in the TPR spectrum was 640 K. The second band was rising from 700 K and the H_2 consumption continuously increased until 1100 K, as shown in Fig. 2. This indicated that some Co could not be reduced at lower temperatures. For the Ru-, Pd-, and Pt-promoted catalysts, the main peaks were located at 600 K, 613 K, and 653 K, respectively while smaller peaks at 300–500 K were supposed to be due to the reduction of cobalt around noble metals. The higher temperature peaks for Ru-, Pd-, and Pt-promoted catalysts were located at 693 K, 973 K, and 983 K, respectively. The peak positions also supported the conclusion that the Ru-promoted catalyst, where Ru was enriched by Co, was very easily reduced. Pt or Pd may form a uniform alloy with Co, but it had little influence on the Co reduction degree.

Catalyst Structure

Table 2 shows the results of the catalyst characterization in terms of the catalyst structure. It is interesting that the H_2 adsorption amount on the catalyst promoted by Pt or Pd was much larger than that on the other two catalysts. The total H_2 uptake by catalysts followed the order

TABLE 2

Characterization of Various Catalysts

Catalyst[a]	Uptake (μmol g^{-1})				Reduction degree[d] (%)	Dispersion[e] (%)	Particle size (nm)			TOF[g]	Cobalt–time yield[h]
	Total H_2[b]		Total CO[c]	Irre. CO[c]			$H_{2(ad)}$[f]	XRD	XRD		
	B	A					R	R	O	$\times 10^2$ s^{-1}	($\times 10^4$ s^{-1})
Co	36.6	37.3	46.3	32.6	50	8.63	12.02	5.94	7.64	8.2	1.86
RuCo	58.6	56.9	93.6	88.9	99.8	6.91	13.09	10.28	6.61	11.1	4.02
PtCo	108.9	104.4	186.7	141.9	56	22.67	4.15	3.12	6.49	4.1	2.75
PdCo	90.4	85.6	145.2	102.1	63	16.62	5.63	4.38	7.38	5.8	3.22

Note. B, before reaction; A, after reaction; R, after reduction; O, before reduction.
[a] After reduction at 673 K.
[b] Adsorption temperature was 373 K.
[c] Adsorption temperature was room temperature.
[d] Assuming the noble metals are completely reduced at 673 K.
[e] Assuming the stoichiometry H_{ad}/Co_s or $M_s = 1$ (M = Ru, Pt, and Pd).
[f] Calculated by $d_s(\text{nm}) = 96/D(\%)$ according to Ref. (18).
[g] TOF was based on the amount of total H_2 uptake.
[h] Cobalt–time yield: moles of CO converted per total gram-atoms of Co per second.

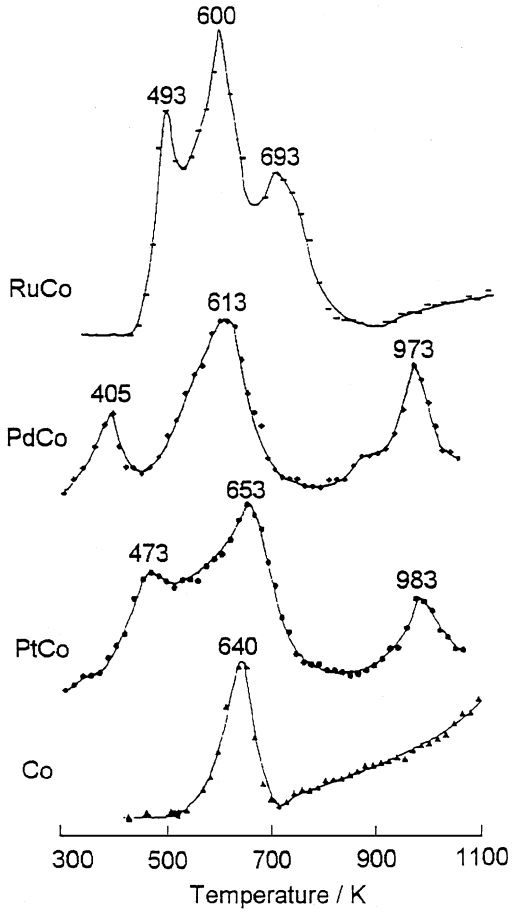

FIG. 2. TPR profiles of Co, PtCo, PdCo, and RuCo catalysts. Heating rate, 7 K min^{-1}; 5% H_2 in argon.

PtCo > PdCo > RuCo > Co. Based on the amount of O_2 consumed by at 673 K, the extent of cobalt oxide reduction was calculated by using the stoichometric formula described below:

$$3Co^0 + 2O_2 \rightarrow Co_3O_4$$

$$Pt^0 + \frac{1}{2}O_2 \rightarrow PtO$$

$$Pd^0 + \frac{1}{2}O_2 \rightarrow PdO$$

$$2Ru^0 + \frac{3}{2}O_2 \rightarrow Ru_2O_3.$$

Here it is assumed that all reduced Co and noble metal species could be oxidized at 673 K, and all noble metal atoms were completely reduced under the pretreatment conditions. Based on this assumption, the degree of reduction of Co in monometallic and bimetallic catalysts was determined, as shown in Table 2. The reducibility of cobalt oxide increased from 50% to 56–99.8% by addition of noble metals. This is one main reason why (M + Co) catalyst exhibited higher activity than Co. The dispersion of catalyst is defined as the ratio of $(Co_s + M_s)/(Co_0 + M_0)$, where Co_s or M_s represents the number of surface Co or noble metal atoms obtained from H_2 adsorption, assuming H/Co_s or H/M_s to be 1. Co^0 or M^0 represents the metallic state Co or noble metals. It should be noted that oxidized cobalt species was not included in the calculation of metal dispersion. This method was used by Chen *et al.* (19). For the Ru-added catalyst, the dispersion decreased. The decrease in dispersion after the addition of Ru may result from a higher concentration of the reduced Co and Ru atoms. However, for the

Pt- and Pd-added catalysts, the dispersions increased remarkably. It is obvious in Table 2 that the reducibility of Pt- and Pd-added catalysts increased only slightly but a large amount of H_2 was adsorbed. Thus, it is clear that Ru increased the cobalt reducibility remarkably; however, Pt and Pd made little contribution to the cobalt reduction. On the other hand, Ru had little effect on the dispersion, while Pt and Pd had a very positive influence on the cobalt metal dispersion. Furthermore, Ru-added catalyst exhibited a large turnover frequency (TOF), but the TOF values of Pt- and Pd-added catalysts were even smaller than that of catalyst Co, as given in Table 2.

The H_2 chemisorption data of the used catalyst after reaction showed that the amount of H_2 adsorption changed little, indicating that most surface cobalt remained in metallic state during the reaction. It seems that under the reaction conditions, H_2O and CO_2 did not oxidize metallic cobalt sites at the surface.

The XRD spectra exhibited only the cobalt peaks, as shown in Fig. 3. No peaks attributed to Ru, Pt, or Pd were observed. The particle size calculated from XRD spectra by Scherrer's equation is shown in Table 2. It is interesting that all of catalysts had nearly the same particle size in the oxide state. However, after reduction, the metallic cobalt particle changed significantly. The metallic cobalt exhibited a narrow and intense peak for Ru-added catalyst, which also provided evidence that Ru-added catalyst had a higher reduction degree and formed large metallic cobalt particles after reduction. This phenomenon should be attributed to the fact that either Ru-added catalyst had a higher reduction degree or Ru induced Co agglomeration during the reduction.

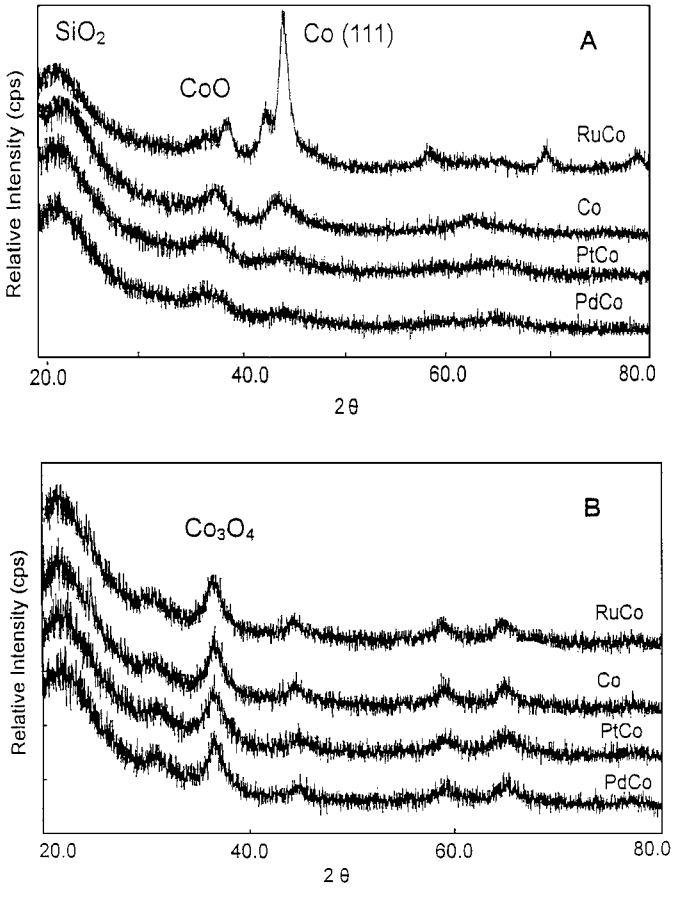

FIG. 3. XRD patterns of Co, RuCo, PtCo, and PdCo. (A) After reduction and (B) before reduction.

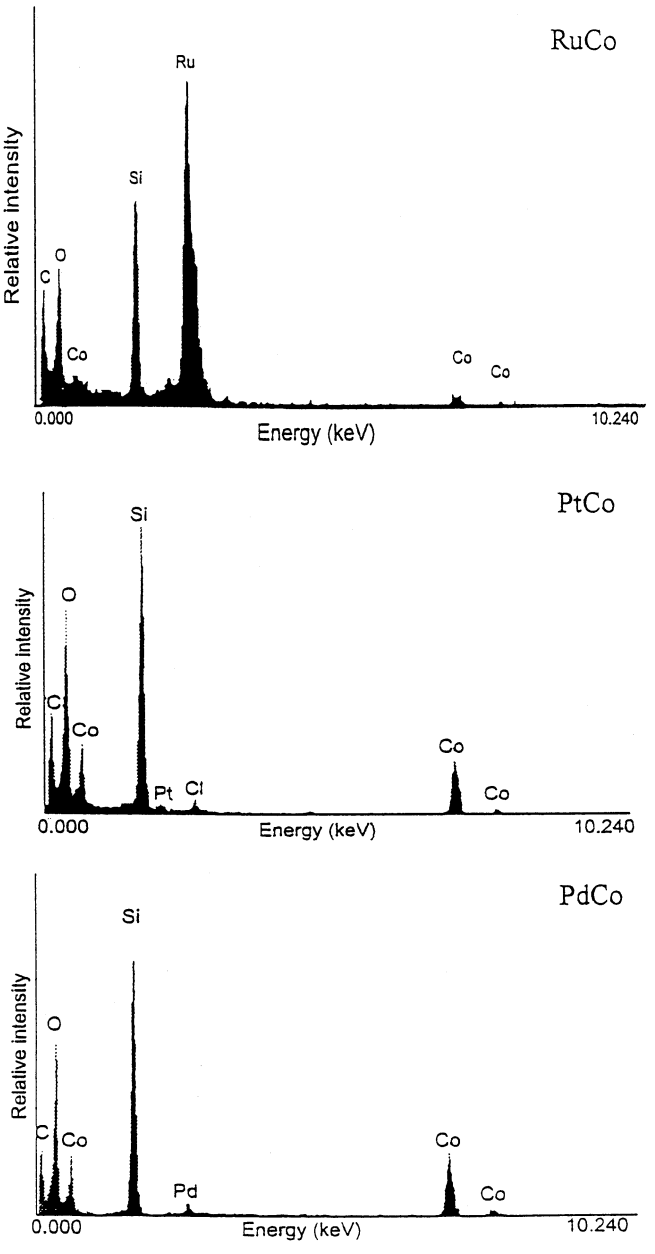

FIG. 4. Energy dispersive spectra obtained for individual metal particles in RuCo, PtCo, and PdCo catalysts. Electron beam size, 0.5 nm.

Individual metallic particles in the bimetallic Ru–Co, Pt–Co and Pd–Co were analyzed by EDS. Representative EDS spectra are given in Fig. 4. The compositions of bimetallic

TABLE 3

Metal Composition in the Alloy as Determined by EDS

Catalyst	Particle no.	Metal composition (at. %)	
		Noble metal	Co
RuCo	1	93.3	6.7
	2	77.7	22.3
	3	85.4	14.6
PtCo	1	5.2	94.8
	2	6.4	93.6
	3	5.1	94.9
PdCo	1	13.2	86.8
	2	7.9	92.1
	3	7.4	92.6

particles resulting from EDS are listed in Table 3. The results gave clear evidence that the noble metals had intimate interactions with Co, and alloys of RuCo, PtCo, and PdCo formed with different compositions. It was found that Ru was very rich in alloy RuCo, compared to its original composition (1.16 mol%). The composition of alloys such as PtCo and PdCo was near the original preparation ratio. It seems that the difference in the composition of the alloys led to changes in the reduction degree and the size of metallic crystalline during catalyst preparation.

TPSR Investigation

In Fig. 5 are shown the TPSR profiles of the catalysts promoted by Ru, Pt, or Pd and only Co. In the case of Co and RuCo catalysts, methane formation began at 360 K and was nearly complete before 460 K. The peaks of methane formation were located at 410 K and 415 K, respectively. However, the peak area for the RuCo catalyst was much larger than that for Co. For the PtCo and PdCo catalysts, methane formation also began at 360 K but was nearly complete at 510 K. The main peak of methane formation was shifted to 430 K and a shoulder peak was located at 410 K. This fact was in very good accordance with the catalytic activity data in Table 1. The peak temperature of CH_4 formation in CO TPSR was reported to be closely related to the catalytic activity of CO hydrogenation (20). The CH_4 peak temperatures of RuCo and Co catalysts were 15 K lower than those of PtCo and PdCo catalysts. This suggests that CO was adsorbed in a more reactive state on the RuCo and Co catalysts than on the PtCo and PdCo catalysts. Thus RuCo and Co showed higher TOF. It is also interesting some of the adsorbed CO on PtCo catalyst desorbed as CO_2, which was not observed on the other three catalysts. CO_2 in TPSR likely comes from two paths: one is the water–gas shift reaction ($CO + H_2O \rightarrow CO_2 + H_2$), as H_2O formed with CH_4, and the other is the Bouodart reaction ($2CO \rightarrow C + CO_2$).

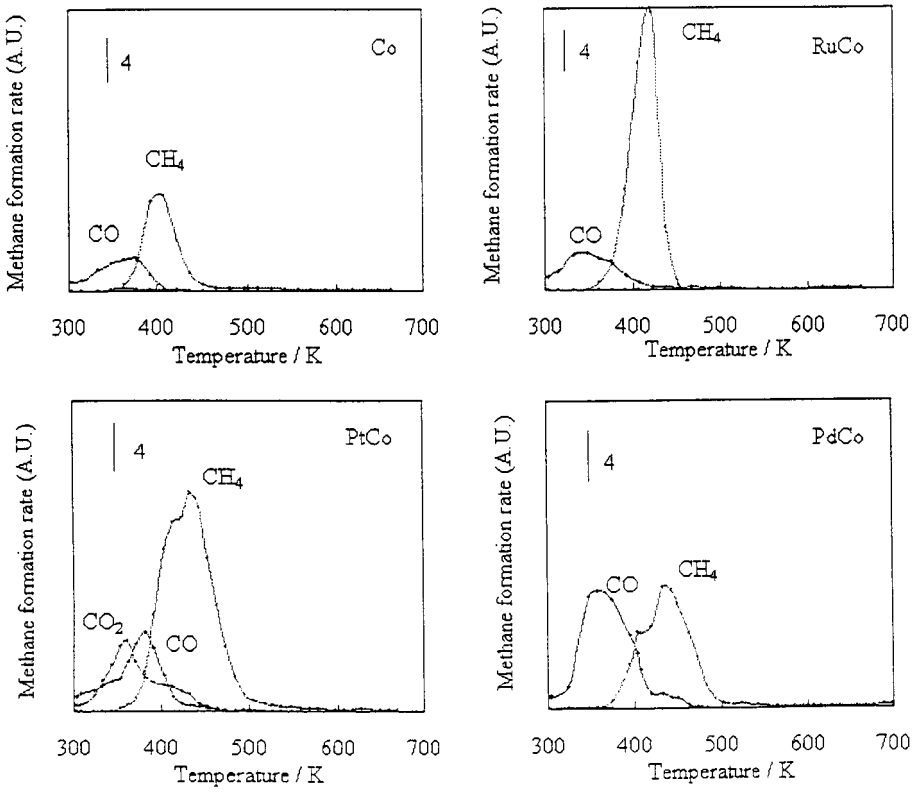

FIG. 5. CO-TPSR spectra of various catalysts after CO adsorption at room temperature.

TABLE 4

Percentage of Adsorbed CO on Various Catalysts Desorbed as CH_4, CO, and CO_2 in TPSR

Catalyst	CH_4/%	CO/%	CO_2/%	CH_4 amount μmol/g-cat.
Co	67.2	32.8	—	21.9
RuCo	78.5	21.6	—	69.7
PtCo	44.2	14.2	41.6	62.7
PdCo	52.4	47.6	—	53.5

TPSR temperature range, 303–673 K; heating rate, 5 K min^{-1}; 100% H_2.

Considering that the peak for CO_2 was located at 360 K, and the methane formation started at 360 K, it seems that CO_2 formation was due to the Bouodart reaction. The catalytic data in Table 1 also show that PtCo catalyst has remarkably higher CO_2 selectivity.

On the Pt- and Pd-added catalysts, the Pt and Pd formed uniform alloys with Co where the particle of Co was small. The geometric effect makes it difficult to cleave the C–O at low temperatures, thus the methane formation peak is located at higher temperatures. On the other hand, the cobalt atoms around Pt or Pd become "electron rich" and the C–O bond on such cobalt atoms was more easily cleaved. So the methane formation peak, appearing as a shoulder peak, was located at lower temperature. This is why Pt- or Pd-added catalyst displayed two methane peaks in their TPSR profiles.

The data in Table 4 showed that more adsorbed CO desorbed as CH_4 at lower temperatures on RuCo catalyst than those on PtCo and PdCo catalysts. It also suggests that RuCo catalyst has a high catalytic activity.

FT-IR Measurement

The transmission FT-IR spectra of the adsorbed CO for the reduced catalysts are compared in Fig. 6. For Co catalyst, an intense peak at 2014 cm^{-1} with two shoulder peaks at 2065, 1943 cm^{-1} and weak peaks at 2181, 1814 cm^{-1} were observed. The 2014 cm^{-1} peak was assigned to CO adsorbed on cobalt metal in a linear geometry (21–24). The 2065 cm^{-1} shoulder peak was assigned to the surface carbonyl species, $Co(CO)_x$ (where $x > 1$), which readily formed at corner sites on the cobalt metal, and the 1943 cm^{-1} shoulder peak was due to the bridge-type CO on Co sites (23, 25). The 1814 cm^{-1} weak peak was assigned to CO adsorbed onto a multifold site (26). The peak at 2181 cm^{-1} was assigned to the CO adsorbed on Co^{n+} ($n = 2, 3$) species (26), as surface cobalt oxide species derived from supported cobalt acetate were difficult to reduce.

For the catalysts PtCo and PdCo, the band for CO adsorbed on cobalt metal in the linear model shifted from 2014 cm^{-1} on Co catalyst to 1997, 2001 cm^{-1}, respectively. Similarly, the peak at 2065 cm^{-1} derived from the surface carbonyl species $Co(CO)_x$ and the peak at 1950 cm^{-1} was from CO in the bridge adsorption state. For the catalyst RuCo, the peak of CO adsorbed as linear type shifted to 2006 cm^{-1}, and the 2065 cm^{-1} peak of $Co(CO)_x$ shifted to 2054 cm^{-1}. The Peak at 1950 cm^{-1}, the bridge-adsorbed CO, was very strong on RuCo. It is believed that bridge-type CO was easily formed on large Co particles here. As has been pointed out, the bridge-type CO was much more active than linear-type CO (20). The high activity of RuCo catalyst could be attributed to the increase in bridge-type adsorbed CO, which was easily dissociated to carbon and oxygen. From EDS, Pt or Pd dispersed very well in cobalt to form an alloy of uniform composition. It is considered that an electronic effect, a kind of legend effect, appeared in PtCo and PdCo catalysts as linear CO peaks of these catalysts shifted remarkably to the lower side, even if the Co particle size decreased. From IR spectra of PtCo and PdCo, a new peak derived from adsorbed CO with the structure between linear and bridge mode might form, resulting in a 1950 cm^{-1} peak in shoulder-peak form. It seems that this electronic effect determined the lower TOF and higher methane selectivity (27). For RuCo, Ru became very rich on the cobalt surface from EDS and bulk cobalt contained little Ru. This might lead to large supported cobalt particles and more bridge-type adsorbed CO. The Legend effect was not so obvious in RuCo as Ru was enriched at the Co particle surface. The shift of the peak for linearly adsorbed CO from 2014 to 2006 cm^{-1} was mainly due to the increase in Co particle size of the RuCo catalyst.

From the viewpoint of particle size effect, the wavenumber of linearly adsorbed CO on PtCo or PdCo should be higher than 2014 cm^{-1}, in analogy to the Co catalyst, as the

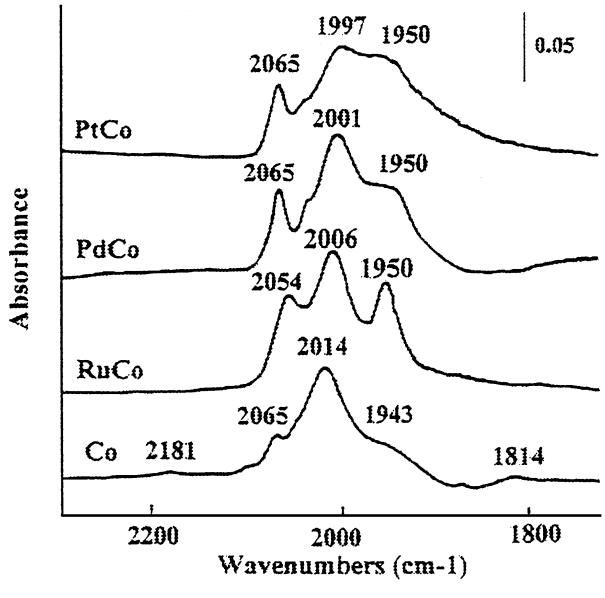

FIG. 6. FTIR spectra of CO adsorbed on various catalysts.

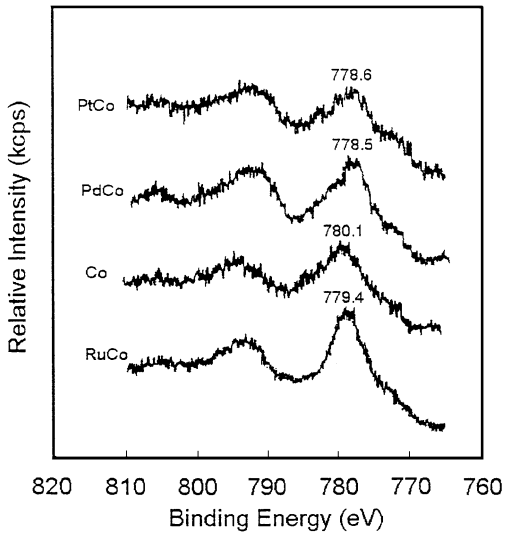

FIG. 7. XPS spectra of cobalt in the noble metal-promoted Co catalyst.

metallic particle size of PtCo and PdCo was smaller than that of the Co catalyst. It is estimated that due to the electronic shift from Pt or Pd to CO, the wavenumber for linear CO on PtCo and PdCo was 1997 and 2001 cm^{-1}, respectively, lower than that of Co catalyst. This electronic effect might also explain why bridge CO on PdCo and PtCo had a stronger peak than that on the Co catalyst.

XPS Analysis

Four catalysts in the reduced state were investigated by XPS. The spectra recorded are shown in Fig. 7. In catalysts Co, RuCo, PtCo, and PdCo, the binding energy (BE) of the $Co_{2p3/2}$ showed peaks at 780.1, 779.4, 778.6, and 778.5 respectively. The $Co_{2p3/2}$ peaks for catalysts PtCo and PdCo appeared at lower positions than that of catalyst Co, indicating that the electron shifted from Pt or Pd to Co. This result was in good accordance with the EDS, TPR, and FT-IR results. For RuCo, the peak of $Co_{2p3/2}$ was sharp. This feature was attributed to the fact that the Co existed in the metallic state. The line shapes of the other three catalysts were broad, providing evidence that the peaks consisted of metallic Co and Co(II) (28). From the O_2 titration data in Table 2, the catalyst RuCo has the highest reduction degree. The BE value of $Co_{2p3/2}$ also showed that Pt and Pd have intimate interactions with cobalt species in these catalysts.

DISCUSSION

It is clear from the evidence above that Ru was enriched at the surface of cobalt crystalline while Pt or Pd formed a nearly uniform alloy with cobalt. During the preparation process, these four catalysts, Co, PtCo, PdCo, and RuCo, exhibited similar XRD patterns until calcinations and only Co_3O_4 peaks were observed, as in Table 2. But after reduction, a sharp peak of metallic cobalt appeared only for RuCo. For the other three reduced catalysts, only very small peaks of unreduced CoO were observed, as shown in Fig. 2. It should be mentioned that the reduced catalyst samples used here were in the passivated form where the reduced bulk metallic cobalt was covered by a tailor-made oxidation membrane before being crushed for XRD measurement. Some cobalt oxides from the membrane might exist besides the originally unreducible cobalt oxide. It is estimated that in the reduced state, Ru–Co alloy with very low Ru concentration was not stable and was liable to separate into different phases: a ruthenium-rich phase as well as a cobalt-rich phase, leading to the formation of a ruthenium-enriched cobalt surface. Only in the oxidation state, could ruthenium or its oxide disperse relatively well in cobalt oxide. Unsupported catalysts of RuCo, PtCo, and PdCo with the same M/Co (M = Ru, Pd, Pt) ratio of the supported catalysts were prepared to ensure great enough peak density to obtain XPS results for the added noble metals. As compared in Table 5, the Ru/Co molar ratio determined from XPS increased from 0.12 in the oxide states to 0.35 in the reduced state even if the Ru/Co molar composition ratio of the RuCo catalyst was 0.012. On the other hand, the Pd/Co ratio was 0.01 and Pt/Co remained 0.005, both in the reduced and oxidized states, respectively. Both of these ratios were very similar to the original composition ratios during the catalyst preparation.

It is well known that Ru is an FT-active metal. From XPS of the silica-supported RuCo, Ru was not detected. But EDS showed that some spots on the surface of the silica-supported RuCo were Ru-rich in structure. From chemisorption and particle size data in Table 2, it is clear that even if RuCo particle size, determined from XRD, increased to be larger than that of the catalyst Co, the CO or hydrogen uptake of RuCo was greatly larger than that of catalyst Co in the chemisorption experiment. From these characterization results, we may say that the main role of Ru itself in RuCo catalyst was reducing cobalt, not contributing FTS activity directly. The Ru-rich spots on the Co surface gave the high reduction degree, as well as large particles, of

TABLE 5

Effect of Reduction and Calcination Treatments on the XPS Peak Intensity Ratio of Noble Metal and Cobalt in the Mixture of Noble Metal and Cobalt

XPS atomic ratio	Oxide state	Reduced state	Original
Ru/Co	0.12	0.35	0.012
Pt/Co	0.005	0.006	0.006
Pd/Co	0.01	0.01	0.011

Calcination temperature, 723 K; reduction temperature, 673 K; XPS peaks, Ru($3d_{3/2,5/2}$), Pt($4f_{7/2,5/2}$), Pd($3d_{3/2,5/2}$) and Co($2p_{1/2,3/2}$). No silica was present.

RuCo and the structure formed during the reduction process of the catalyst preparation.

The formation of alloy may be determined by its thermodynamics or phase equilibrium. From the viewpoint of catalysis, the explanation is that hydrogen activated at Ru-rich spots on the RuCo surface reduced cobalt, including the finely dispersed cobalt oxide from cobalt acetate, effectively. As Iglesia pointed out, mobile RuO_x formed easily during the oxidation (29). The effect of Ru on cobalt oxide reduction was enhanced by reduction–oxidation cycles that promoted bimetallic mixing. This kind of mobile RuO_x became rich at the surface of cobalt oxide, as clearly shown in the XPS results for unsupported RuCo catalysts in Table 5. High reduction degree might also result in sintering-like particle increase during the reduction process.

If a unified material, such as only Ru, or PdCo or PtCo in this research, is used, of course, the higher the dispersion, the lower the TOF. But in the low dispersion/large particle case, the overall CO conversion will be low. RuCo in this paper exhibited the highest CO conversion and the biggest particle size meantime. It is clear that the geometric explanation alone is not enough to elucidate the behavior of RuCo with both electronic interaction between Ru–Co and un-uniform spatial distribution of Ru.

In Table 6, the effect of reduction temperature on the RuCo catalyst activity was shown. When the reduction temperature increased from 473 to 673 K, the degree of reduction of the catalyst and CO apparent conversion were enhanced. The cobalt–time yield also increased with the reduction temperature. But the TOF was nearly the same, indicating that FTS under these conditions was structure-insensitive. By comparing the catalysts reduced at 673 and 773 K, it is clear that the latter exhibited a larger TOF. As all the cobalt oxide was reduced on both catalysts, it is inferred that too high a reduction temperature led to supported metallic crystalline sintering to some extent and the TOF was increased, after FT metal oxide was completely reduced. In this way, FTS was structure-sensitive sometimes.

TABLE 6

Effect of Reduction Temperature on the RuCo Catalyst Activity

Reduction temperature (K)	CO conversion (%)	Reduction degree (%)	Cobalt–time yield[a] ($\times 10^4$ s^{-1})	TOF ($\times 10^{-2}$ s^{-1})
473	30.2	41.7	1.68	11.0
573	50.9	70.2	2.84	10.9
673	72.3	99.8	4.02	11.1
773	69.2	99.9	3.84	12.3

Reaction conditions: 513 K, 1.0 MPa, $CO/H_2 = 1/2$, $W/F = 5$ g-cat. h mol^{-1}; total cobalt loading, 10 wt%; Ru loading, 0.2wt%; reduction time, 10 h. TOF was obtained by the method described in Table 2.

[a] Cobalt–time yield: moles of CO converted per total gram-atoms of Co per second.

For the Co/SiO_2 catalysts prepared from mixed precursors of cobalt acetate and cobalt nitrate, without noble metal addition, it has been reported that TOF was the same for all catalysts with different acetate-to-nitrate ratios (9). Considering the fact that all the mixed-precursor-derived catalysts without noble metal addition had less than 100% reduction degree, FTS was structure-insensitive, in accordance with the facts here.

The enrichment of Ru metal at the cobalt surface made gaseous hydrogen, which was activated more easily on Ru to reduce the cobalt oxide effectively during the catalyst reduction (8). Consequently, the degree of reduction of cobalt was very high as shown in Table 2. It is also considerable that the high degree of reduction of cobalt made the metallic cobalt crystal growth effectively, as no cobalt oxide phase could stop the sintering of cobalt metal phase. In contrast, Pd or Pt highly dispersed in the alloy could not form large bulk noble metal crystalline and the concentration of the noble metals at the surface of cobalt was lower than 1%. More importantly, Pd or Pt atoms in the form of alloys of this kind of composition lost their original metallic property. As indicated in XPS results in Fig. 7, due to the electron shift from noble metal to cobalt, it is clear that noble metal existed in a cation-like state, especially for Pd and Pt. This kind of valency change made Pt and Pd less effective for hydrogen activation, in some extent, both in catalyst reduction in the preparation process and in the FTS reaction itself. Based on the assemble effect as well as the legend effect of the PdCo and PtCo alloys, the reduction degree was low and the cobalt particle size was small.

As seen in Fig. 1, the effect of ruthenium addition did not need high concentration of ruthenium. While the molar ratio of $Ru/(Ru + Co)$ was higher than 2%, no significant change in the catalyst performances was observed. From the structure of the catalyst RuCo, it is clear that a concentration of Ru higher than 2% would not be effective to further increase the reduction degree of the cobalt and the hydrogen activation step was not the rate-determining step in the whole FTS reaction network. It is also estimated that if the ruthenium composition was further enhanced, the cobalt particle size would not be increased.

From the IR observation, bridge-adsorbed CO appeared to a large extent on RuCo which is generally considered as more reactive adsorbed CO. Due to the large crystalline size of cobalt in the RuCo catalyst, more flat cobalt surfaces could be provided to form bridge-type CO (30). This feature determined the high activity of RuCo. From Table 1, the chain growth probability of RuCo was slightly larger than those of PtCo and PdCo, which agreed well with the observation of Nils and Jacobs (30). Large supported metal favored carbon chain growth, as indicated also by Kellner and Bell (31). As this reaction was conducted in a semi-batch flow-type reactor, hydrocarbons formed, especially the heavier one, readily stayed inside the reactor to undergo

secondary hydrocracking. It was not easy to obtain an obvious difference in the chain growth probability among these three catalysts. If the reaction used a gas-phase reactor, a more distinct difference in the chain growth probability would appear (32).

Compared to other catalysts in Table 1, noble-metal-added catalysts showed lower chain growth probability. One reason was the strong ability to hydrogen activate the noble metal, which introduced much hydrogen to the catalyst surface, enhancing methane formation as in Table 4 and suppressing the carbon-chain growth process. The other reason was the existence of acetate-derived cobalt crystalline with very small size (10). For either the ruthenium-added catalysts or the nonaddition catalysts, the chain growth probability of the catalyst from the mixture of acetate and nitrate was lower than that of the catalyst from nitrate only. As the cobalt metallic crystalline reduced from acetate was very small, the observed overall carbon-chain growth probability of the catalyst with dual cobalt precursors was low. It seems that a part of the acetate-derived cobalt existed separately, without sintering or combination with nitrate-derived large cobalt metals.

From the TPR patterns in Fig. 4, it is clear that besides the main peaks, peaks on the low-temperature side, centered at 493 K, 405 K, and 473 K, also appeared in spectra of the noble-metal-added catalysts, which were assigned to the reduction of cobalt oxides near the noble metal, supporting the conclusion above that noble metal accelerated the hydrogen diffusion from the gas phase to the catalyst surface. Furthermore, the high-temperature peak for Co catalyst distributed between 700 K and 1100 K was from the acetate-derived oxide. With the noble metal addition, this peak shifted to 693 K, 973 K, and 983 K, respectively. Noble metal promoted the reduction of these highly dispersed fine cobalt oxides. Especially ruthenium showed a very remarkable promotional effect. Because all the catalysts were reduced at 673 K during the preparation, only on RuCo, almost all the cobalt species was reduced. Some of the acetate-derived cobalt oxide could not be reduced on PtCo, PdCo, and Co during catalyst preparation. This observation was in accordance with the reduction degree results in Table 2.

Concerning the TPSR peaks in Fig. 5, RuCo exhibited a lower methane peak temperature than PdCo and PtCo, as determined from the large amount of bridge-type-adsorbed CO on RuCo catalyst. Although Co catalyst also had a methane peak at low temperature, the methane peak area on RuCo was significantly larger than that on Co. The reason for this phenomenon was that the degree of reduction of the supported cobalt and amount of reactive adsorbed CO were higher on RuCo, as shown in Fig. 6. The shoulder peaks at the lower temperature side of the methane peaks of PtCo and PdCo were considered to be from the CO adsorbed onto the cobalt adjacent Pd or Pt, as this cobalt was easily reduced and might receive an electron from Pd or Pt.

From the hydrogen adsorption of the fresh and the used forms of these four catalysts, as in Table 2, the reduction degree and the dispersion were not changed during the FTS reaction. Although FTS produced a lot of water as well as CO_2, it is clear that the reduction state of cobalt did not change. Noble metal and large cobalt crystalline introduced hydrogen from syngas to the catalyst surface to maintain the reduction state during the FTS reaction. Moreover, it is considered that water could not stay inside the catalyst micropores which were filled by the produced hydrocarbons and reaction medium oil, due to the low affinity between water and hydrocarbons. This effect prevented metallic cobalt from being oxidized by water.

CO transportation restrictions must be considered carefully, especially in the slurry-phase FTS. The present reaction conditions were well selected to avoid a possible diffusion-controlled regime, as reported in another paper (33). The apparent activation energy for the catalysts here was about 17 kcal/mol to 18 kcal/mol, near those values reported in an FTS review (34). So the influence of diffusion of CO was not very severe here. The pellet size was 0.075 mm (200 mesh). The mean pore size of the obtained catalyst was around 8.0 nm. And the void fraction of the pellet was 0.61. With the calculation method reported by the present authors (35), the catalyst effectiveness factors for Table 1 were 0.90–0.96, indicating that a CO diffusion-controlled mechanism did not work.

CONCLUSIONS

(1) Although Co catalyst prepared from mixing cobalt nitrate and cobalt acetate had a high activity for the CO hydrogenation, the addition of a very small amount of noble metal such as Ru increased the catalyst activity effectively. The catalytic activity of noble-metal-promoted Co catalysts followed the order RuCo > PtCo > PdCo > Co. (2) The added noble metals had a significant effect on the methane selectivity. Pt- and Pd-added catalysts showed high methane selectivity, which was attributed to the small metallic cobalt particle and H_2 spillover effect. (3) Ru improved Co reducibility greatly but had only a slight effect on Co dispersion. Pt and Pd increased the Co reducibility slightly but significantly influenced Co dispersion and turnover rate. (4) The EDS, TPR, and XPS results confirmed that noble metals and cobalt interacted intimately. Pd and Pt formed well-dispersed alloys with Co, while Ru formed two distinct phases where Ru was enriched at the Co surface. This kind of structure variance determined the different reaction behavior of PtCo, PdCo, and RuCo catalysts. (5) Pd and Pt in the alloy with Co provided electrons to cobalt, leaving themselves less H_2 activation ability. (6) Before the supported cobalt

catalyst was completely reduced, the FTS reaction was structure-insensitive. But for the supported metallic catalyst, this was not the case. (7) The Ru-rich spots on the Co surface determined the high reduction degree, as well as large particle size of RuCo and this structure formed during the reduction step of the catalyst preparation. Most of the Pd and Pt was embedded in the bulk phase of Co or CoO_x, not contributing to the reduction of supported cobalt oxides.

ACKNOWLEDGMENTS

This work was partially supported by JSPS (RFTF98P01001), NEDO (Contract No. 97E10005), and a Sasakawa Scientific Research Grant from The Japan Science Society.

REFERENCES

1. Anderson, R. B., "The Fischer-Tropsch Synthesis." Academic Press, New York, 1984.
2. Haggin, J., *Chem. Eng. News* **23** (July), 27 (1990).
3. Iglesia, E., Soled, S. L., and Fiato, R. A., *J. Catal.* **137**, 212 (1992).
4. Johnson, B. G., Bartholomew, C. H., and Goodman, D. W., *J. Catal.* **128**, 231 (1991).
5. Soled, S. L., Baumgartner, J. E., Reyes, S. C., and Iglesia, E., *Proc. Mater. Res. Soc. Symp.* **368**, 113 (1995).
6. Takeuchi, K., Matsuzaki, H., Arakawa, H., Hanaoka, T., and Sugi, Y., *J. Mol. Catal.* **55**, 361 (1989).
7. Matsuzaki, T., Takeuchi, K., Hanaoka, T., Sugi, Y., and Reinikainen, M., *Catal. Lett.* **10**, 193 (1991).
8. Matsuzaki, T., Takeuchi, K., Hanaoka, T., Arakawa, H., and Sugi, Y., *Catal. Today* **28**, 251 (1996).
9. Sun, S. L., Tsubaki, N., and Fujimoto, K., *Appl. Catal.* **202**, 121 (2000).
10. Sun, S. L., Fan, L., and Fujimoto, K., *Chem. Lett.* 343 (1999).
11. Zsoldos, Z., Hoffer, T., and Guczi, L., *J. Phys. Chem.* **95**, 795 (1991).
12. Iglesia, E., Soled, S. L., Fiato, R. A., and Via, G. H., *J. Catal.* **143**, 345 (1993).
13. Guczi, L., Hoffer, T., Zsoldos, Z., Zyade, S., Maire, G., and Garin, F., *J. Phys. Chem.* **95**, 802 (1991).
14. Zsoldos, Z., and Guczi, L., *J. Phys. Chem.* **96**, 9393 (1992).
15. Schanke, D., Vada, S., Blekkan, E. A., Hilmen, A. M., Hoff, A., and Holmen, A., *J. Catal.* **156**, 85 (1995).
16. Zowtiak, J. M., and Bartholomew, C. H., *J. Catal.* **83**, 107 (1983).
17. Chin, R. L., and Hercules, D. M., *J. Phys. Chem.* **86**, 360 (1982).
18. Reuel, R. C., and Bartholomew, C. H., *J. Catal.* **85**, 63 (1984).
19. Chen, Y. G., Tomishige, K., Yokoyama, K., and Fujimoto, K., *Appl. Catal.* **165**, 335 (1997).
20. Fujimoto, K., Kameyama, M., and Kunugi, T., *J. Catal.* **61**, 7 (1980).
21. Sato, K., Inoue, Y., Kojima, I., Miyajaki, E., and Yasumori, I., *J. Chem. Soc., Faraday Trans. 1* **80**, 841 (1984).
22. Mohana, K. R., Spoto, G., and Zecchina, A., *J. Catal.* **113**, 466 (1988).
23. Dees, M. J., Schidi, T., Iwazawa, Y., and Ponec, V., *J. Catal.* **124**, 530 (1990).
24. Lapidus, A., Krylova, A., Kazanskii, V., Borovkov, V., Zaitsev, A., Rathousky, J., Zukal, A., and Jancalkova, M., *Appl. Catal.* **73**, 65 (1978).
25. Heal, M. J., Leisegang, E. C., and Torrington, R. G., *J. Catal.* **51**, 314 (1978).
26. Ischi, S., Ohno, Y., and Viswanathan, B., *Surf. Sci.* **161**, 349 (1985).
27. Vannice, M. A.,"Catalysis, Science and Technology," Vol. 3. Spinger-Verlag, Berlin, Heidelberg, New York, 1982.
28. Chuang, T. J., Brundle, C. R., and Rice, D. W., *Surf. Sci.* **59**, 413 (1976).
29. Iglesia, E., *Appl. Catal. A* **161**, 59(1997).
30. Nijs, H. H., and Jacobs, P. A., *J. Catal.* **65**, 328 (1980).
31. Kellner, C. S., and Bell, A. T., *J. Catal.* **75**, 251 (1982).
32. Fan, L., Yokota, K., and Fujimoto, K., *Topics Catal.* **2**, 267 (1995).
33. Sun, S., Tsubaki, N., and Fujimoto, K., *J. Chem. Eng. Jpn.* **33**, 232 (2000).
34. Van Der Laan, G. P., and Beenackers, A., *Catal. Rev. Sci. Eng.* **41**, 255 (1999).
35. Fan, L., Yokota, K., and Fujimoto, K., *AIChE J.* **38**, 1639 (1992).